Highly selective mercury(II) cations detection in mixed-aqueous media by a ferrocene-based fluorescent receptor

ARTICLE *in* DALTON TRANSACTIONS · FEBRUARY 2012

Impact Factor: 4.2 · DOI: 10.1039/c2dt12156e · Source: PubMed

Dalton Transactions

Dynamic Article Links

Cite this: *Dalton Trans.*, 2012, **41**, 4437

www.rsc.org/dalton

PAPER

Highly selective mercury(II) cations detection in mixed–aqueous media by a ferrocene-based fluorescent receptor†

María Alfonso,[a] Julia Contreras-García,[b] Arturo Espinosa,[a] Alberto Tárraga*[a] and Pedro Molina*[a]

Received 11th November 2011, Accepted 16th January 2012
DOI: 10.1039/c2dt12156e

A new chemosensor molecule **3** based on a ferrocene–imidazophenanthrophenazine dyad effectively recognizes Hg^{2+} in an aqueous environment through three different channels. Upon recognition, an anodic shift of the ferrocene–ferrocenium oxidation potential ($\Delta E_{1/2}$ = 240 mV) and a progressive red shift ($\Delta\lambda$ = 17 nm) of the low energy band in its absorption spectrum is produced. The emission spectrum of **3** in an aqueous environment, CH_3CN–EtOH–H_2O (65 : 25 : 10), and conducted at pH = 7.4 (20×10^{-3} M HEPES) (Φ = 0.003), is perturbed after addition of Hg^{2+} cations and an intense and structureless red shift emission band at 494 nm ($\Delta\lambda$ = 92 nm) appeared along with an increase of the intensity of the emission band (CHEF = 77), the quantum yield (Φ = 0.054) resulted in a 18-fold increase. The combined ^{1}H NMR data of the complex and the theoretical calculations suggest the proposed bridging coordination mode.

Introduction

Selective molecular sensing of metal ions continues to be a practical research aim in both biological and environmental chemistry. As the third most frequently found and second most common toxic heavy metal in the list of the Agency for Toxic Substances and Disease Registry (ATSDR) of the U.S. Department of Health and Human Services, the mercury ion (Hg^{2+}) poses a huge threat to human beings and the environment due to its bioaccumulation, its ability to cause permanent damage, and its long residence in central nervous and endocrine systems.[1] Typically, mercury exists in inorganic forms or as organic mercury compounds. As the most prevalent inorganic form, after entering the aquatic ecosystem, Hg^{2+} is biomethylated *in situ* by microorganisms and converted into its organic form, which is then readily absorbed by fish and eventually accumulated through the trophic chain.[2] The concentration of this ion is therefore the object of strict regulation and should not exceed 1 μg L^{-1} in drinking water.[3] Traditional analytical techniques for Hg^{2+} include atomic absorption spectroscopy, cold vapor atomic fluorescence spectrometry and gas chromatography. These methods, however, require not only complicated instrumentation but also a long measuring time. Therefore, it is urgent to develop new methods for monitoring Hg^{2+} with a low limit of detection, as well as rapid and facile detection. Monitoring of the mercury level in drinking water and food can be aided significantly by small molecule dyes that are structurally engineered with metal binding sites to function as chemosensors.[4] Fluorescence is a sensitive technique. It often relates to various soluble organic-based molecules that are planar, rigid, and π-delocalized and is even scalable to where the emissions of single molecules can be detected. Methods based on fluorescent molecular probes have attracted considerable interest because of the high sensitivity, easy visualization and short response time for detection of the fluorescence signal.[5] Molecular and ionic recognition involving "turn-on" fluorescence intensity with Hg^{2+} is also challenging because of its quenching nature. Thus, considerable efforts have been devoted to the design of fluorescent probes for Hg^{2+} cations.[6]

Ferrocene-based ligands have been found to be useful for incorporating redox functions into supramolecular complexes to bind and allow the electrochemical sensing of cations, anions, and neutral molecules by change in the oxidation potential of Fe(II)–Fe(III) redox couple.[7] In this context, we have found that a number of ferrocene–azaheterocycle dyads selectively sense transition metal cation through several channels.[8] Recently, new chemosensor molecules based on ferrocene–imidazoquinoxalines have been reported, which effectively recognize transition metal cations in acetonitrile solutions.[9] With these considerations in mind, we decided to annulate an additional pyrene ring, which has often been used as an effective fluorescence probe, to the imidazoquinoxaline core, and which could also impart interesting photophysical properties. In this context, the polycyclic receptor **3** has been chosen to develop a multichannel system, where the fluorescent reporter is integrated with and the redox unit is linked to the guest cation binding site.

[a]*Departamento de Química Orgánica, Universidad de Murcia, Campus de Espinardo, 30100 Murcia, Spain. E-mail: pmolina@um.es, atarraga@um.es; Fax: +34 968 364 149; Tel: +34 968 367 496*
[b]*Laboratoire de Chimie Théorique, Université Pierre et Marie Curie, 75005 Paris, France*

†Electronic supplementary information (ESI) available: NMR spectra. Electrochemical data. Emission and ^{1}H NMR titration data. ESI-MS spectra. Detection limit calculations. General comments. Computational details. Energy and Cartesian coordinates for all computed species and additional NCI plots. See DOI: 10.1039/c2dt12156e

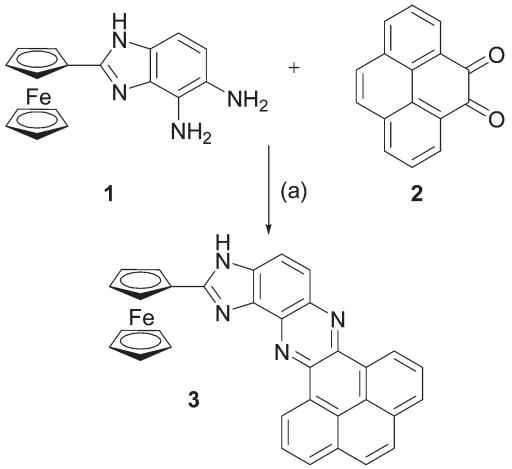

Scheme 1 Synthesis of receptor **3**. *Reagents*: (a) $C_6H_5NO_2$, AcOH, 60 °C (35%).

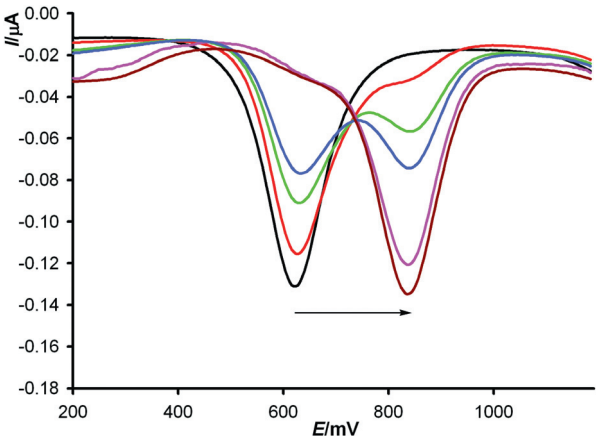

Fig. 1 Evolution of the OSWV of **3** (1×10^{-4} M) in CH_3CN/[(n-Bu)$_4$]PF_6 scanned at 0.1 V s^{-1} in the presence of increasing amounts of Hg$(OTf)_2$, from 0 (black) to 0.5 equiv. (deep red).

Results and discussion

Synthesis

The target receptor **3** was prepared by condensation of the diaminoferrocenylimidazole[9c] **1** with pyrene-4,5-dione **2**, available by oxidation of pyrene with the system ruthenium(III) chloride and sodium periodate in CH_3CN at room temperature.[10] The structure of this new receptor was confirmed by means of standard spectroscopic techniques (^{1}H and ^{13}C NMR), electrospray mass spectrometry (ESI MS), and elemental analyses, all data being in agreement with the proposed structure (Scheme 1).

Cation binding studies

The complexing properties of receptor **3** toward various metal cations (Li^+, Na^+, K^+, Ca^{2+}, Mg^{2+}, Ni^{2+}, Cu^{2+}, Zn^{2+}, Cd^{2+}, Hg^{2+}, and Pb^{2+}), added as their triflate or perchlorate salts have been investigated by electrochemistry, spectroscopic measurements, and ^{1}H NMR spectroscopy.

The redox chemistry of compounds **3** was investigated by linear sweep voltammetry (LSV), cyclic voltammetry (CV), and Osteryoung square wave voltammetry (OSWV) in a CH_3CN solution ($c = 1 \times 10^{-4}$) containing 0.1 M [(n-Bu)$_4$N]PF_6 as supporting electrolyte. As expected, receptor **3** displays a reversible one-electron oxidation process at $E_{1/2}$ = 0.62 V *versus* decamethylferrocene, due to the ferrocene–ferrocenium redox couple. The criteria applied for reversibility were: (i) separation of 60 mV between cathodic and anodic peaks, (ii) close-to-unity ratio of the intensities of the cathodic and anodic currents, and (iii) constancy of the peak potential on changing sweep rate in the CVs. Likewise, the OSWV also exhibits the oxidation peak at the same potential observed in the corresponding CV (see the ESI†).

Titration studies were carried out by using LSV, and OSWV.[11] Thus, addition of the above-mentioned set of metal cations to an electrochemical solution of receptor **3** ($c = 10^{-4}$ M) in CH_3CN containing $TBAPF_6$ (0.1 M) as supporting electrolyte demonstrate that the stepwise addition of substoichiometric amounts of Hg^{2+} promotes the gradual appearance, in the OSWV, of a new oxidation peak at a more positive potential ($E_{1/2}$ = 0.86 V, $\Delta E_{1/2}$ = 240 mV) associated with the formation of a complexed species (Fig. 1). The current intensity of this new peak increases until 0.5 equiv. of the guest cation is added. At this point, the peak corresponding to the uncomplexed receptor **3** disappears. On the other hand, while addition of Zn^{2+} also caused a noticeable but small anodic shift of the oxidation potential ($\Delta E_{1/2}$ = 30 mV) (ESI†), the other metal ions tested (Li^+, Na^+, K^+, Ca^{2+}, Mg^{2+}, Ni^{2+}, Cd^{2+}, and Pb^{2+}) had no effect neither on the LSV nor on the CV or OSWV of this receptor, even when present in a large excess.

A special behavior is observed upon addition of Cu^{2+} to the CH_3CN solution of this receptor because Cu^{2+} behaves as an oxidizing agent toward ferrocene[12] with its concomitant reduction to Cu^+. Thus, LSV studies carried out upon addition of Cu^{2+} to the CH_3CN electrochemical solutions of receptor **3** showed a significant shift of the sigmoidal voltammetric wave toward cathodic currents, indicating that this metal cation promotes the oxidation of the free receptors (Fig. S4†). This oxidation process was also confirmed by comparison of the absorption spectrum resulting from the electrochemical oxidation of **3** and that obtained upon addition of Cu^{2+} metal ions (ESI†). By contrast, the same experiments carried out upon addition of Zn^{2+} and Hg^{2+} metal cations to receptor **3** revealed a shift of the linear sweep voltammogram toward more positive potentials, which is in agreement with the complexation process previously observed by OSWV (ESI†).

One of the most important attributes of receptor **3** is the presence of a ferrocene moiety in proximity of the cation-binding nitrogen atoms. Previous studies on ferrocene-based ligands have shown that their characteristic low energy (LE) bands in the absorption spectra are perturbed upon complexation.[13] Therefore, the metal recognition properties of the receptor **3** toward the above-mentioned set of metal cations were also evaluated by UV-vis spectroscopy in CH_3CN. The absorption spectrum of receptor **3** is characterized by strong high energy (HE) absorptions at 307 nm (ε = 19 980 M^{-1} cm^{-1}), 327 nm (ε = 1625 M^{-1} cm^{-1}), and 349 nm (ε = 1410 M^{-1} cm^{-1}). In addition to these bands, another weaker LE band is visible at 433 nm (ε = 500

M^{-1} cm^{-1}) which is assigned to a localized excitation with a lower energy produced by two nearly degenerate transitions, an Fe(II) d–d transition,[14] or a metal-to-ligand charge transfer (MLCT) process (dπ–π*).[15] The optical detection capability of receptor **3** toward the above mentioned set of metal cations, upon addition of increasing amounts of such ions to a CH_3CN solution ($c = 5 \times 10^{-5}$ M) of this receptor, demonstrates that only the presence of Hg^{2+}, Pb^{2+} and Zn^{2+} cations displayed modifications of the UV-vis spectrum of the free ligand (ESI†). By contrast, addition of the other metal cations did not generate significant changes in the UV-vis spectra of the free ligand. These results parallel with those obtained from the electrochemical studies previously described. Job's plot and titration profiles measured by UV-vis spectrophotometry (ESI†) indicated that receptor **3** binds Hg^{2+}, Pb^{2+}, and Zn^{2+} cations in a 2 : 1, 1 : 1, and 1 : 1 fashion, respectively. The calculated global association constants, by using the computer program Specfit/32,[16] gave rise to values of $\beta = 6.37 \times 10^{10}$ M^{-2}, for Hg^{2+}, 1.74×10^{6} M^{-1} for Pb^{2+}, and 1.58×10^{3} M^{-1} for Zn^{2+}.

Cation affinities were also determined through the extent to which the fluorescence intensity of receptor **3** was affected in the presence of the selected metal cations. Receptor **3** exhibits a very weak fluorescence in CH_3CN ($c = 1 \times 10^{-5}$ M) when excited at $\lambda_{ex} = 300$ nm, the emission spectrum showing two weak and well-defined emission bands at 382 and 402 nm, ascribed to the monomeric emission with a rather low quantum yield ($\Phi = 1 \times 10^{-3}$). The low fluorescence shown by the free receptor results from the efficient photoinduced electron transfer (PET) quenching of the excited estate of the pyrene moiety by the lone pair of the nitrogen atoms in the fused phenazine unit. It is note worthy that while addition of Li^+, Na^+, K^+, Ca^{2+}, Mg^{2+}, Ni^{2+}, Cu^{2+} and Cd^{2+} exhibited basically no discernible changes at all, even when they are present in high concentrations (*i.e.*, 100-fold excess), addition of Zn^{2+}, Pb^{2+} and Hg^{2+} promotes not only the appearance of the typical pyrene excimer emission but also a sizable chelation enhanced fluorescence (CHEF).[17] In fact, the CHEF values obtained were 33 for the case of **3**·Zn^{2+} (Φ = 0.025), 42 for the case of **3**·Pb^{2+} ($\Phi = 0.033$) and 44 for the case of **3**·Hg^{2+} ($\Phi = 0.051$). The observed enhancement in the fluorescence intensity (ESI†) can be associated to the reversal of the PET effect which should take place when the metal cations are bound to the nitrogen atoms of the heterocyclic moieties.

The sensing capability of **3** towards the above mentioned set of metal cations was also evaluated and analyzed quantitatively in CH_3CN–EtOH (70 : 30) solutions of this receptor by using UV-vis and emission spectroscopies. It is worth mentioning that both the absorption and emission spectra of receptor **3** obtained in this mixed organic solution did not show any significant change with reference to those obtained in pure CH_3CN solvent. Nevertheless, the titration experiments carried out under these conditions revealed that only the addition of Hg^{2+} metal cations promotes significant changes in the absorption and emission spectra of the free receptor, which indicates that the selectivity of **3** can be modulated by the use of the appropriate organic solvent. Thus, addition of increasing amounts of Hg^{2+} cations to a solution of receptor **3** ($c = 5 \times 10^{-5}$ M) caused a progressive red shift of the LE band to 451 nm ($\varepsilon = 460$ M^{-1} cm^{-1}). These changes occur at approximately three well-defined isosbestic points at $\lambda = 250$, 269, and 445 nm at any receptor–Hg^{2+} ratio,

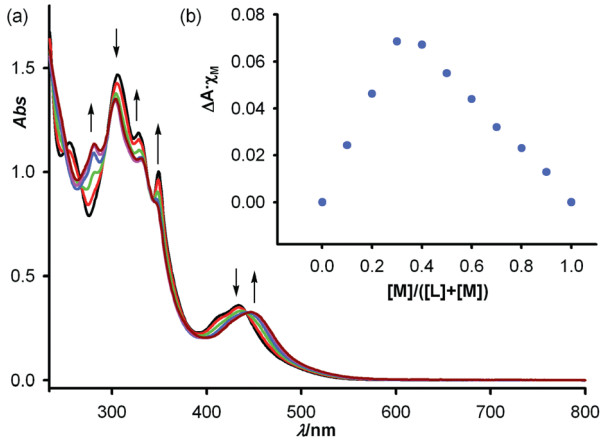

Fig. 2 (a) Changes in the absorption spectra of **3** ($c = 5 \times 10^{-5}$ M in CH_3CN–EtOH (7 : 3)) upon addition of increasing amounts of Hg $(OTf)_2$, from 0 (black) to 0.5 equiv. (deep purple). Arrows indicate absorptions that increase or decrease during the experiment. (b) Job's plot for **3** ($c = 1 \times 10^{-4}$ M in CH_3CN–EtOH (7 : 3)) and $Hg(OTf)_2$ (1×10^{-4} M in CH_3CN–EtOH (7 : 3)), indicating the formation of a 2 : 1 complex.

suggesting that only one complex was formed. The new LE band is red-shifted by $\Delta\lambda = 17$ nm (Fig. 2a). Accurate values of the association constant were determined by using standard UV-titration methods and the above mentioned Specfit program. The binding isotherms were generated by recording the changes in the UV absorption as a function of Hg^{2+} cation concentration. Binding assays using the method of continuous variations (Job's plot) are consistent with a 2 : 1 (receptor : metal) binding stoichiometry (Fig. 2b). The data were well fitted to a 2 : 1 binding isotherm, and the global association constant in this mixed organic solvent was also calculated: $\beta = 7.36 \times 10^{10}$ M^{-2}.

Receptor **3**, when excited at $\lambda_{ex} = 300$ nm, also exhibits a very weak fluorescence in CH_3CN–EtOH (70 : 30) ($c = 1 \times 10^{-5}$ M) ($\Phi = 1 \times 10^{-3}$). In this spectrum, the previously mentioned emission bands ascribed to the monomeric emission of the pyrene unit are present. Fluorescent titration experiments demonstrate that only Hg^{2+} induced a progressive appearance of a redshifted ($\Delta\lambda = 83$ nm) and intense emission band at 485 nm, CHEF = 37, probably due to the excimer fluorescence (ESI†). The stoichiometry of the complex was also determined by the changes in the fluorogenic response of receptor **3** in the presence of varying concentrations of this metal cation, and the results indicate the formation of a 2 : 1 complex with a global association constant of $\beta = 7.91 \times 10^{10}$ M^{-2}, which is in agreement with the one determined by UV-vis titration experiments. On the other hand, the calculated detection limit was in the range of 10^{-6} M. The increase in quantum yield induced by Hg^{2+} ($\Phi = 0.036$), ions was 36-fold. Most remarkable is the fact that the fluorescent response toward Hg^{2+} is preserved in the presence of water. When this study was carried out in an aqueous environment, CH_3CN–EtOH–H_2O (65 : 25 : 10), and conducted at pH = 7.4 (20 mM HEPES) ($\Phi = 0.003$), the addition of Hg^{2+} cations induced the appearance of an intense and structureless red shift emission band at 494 nm ($\Delta\lambda = 92$ nm) and an increase of the emission band's intensity (CHEF = 77), the quantum yield (Φ = 0.054) resulting in a 18-fold increase (Fig. 3).

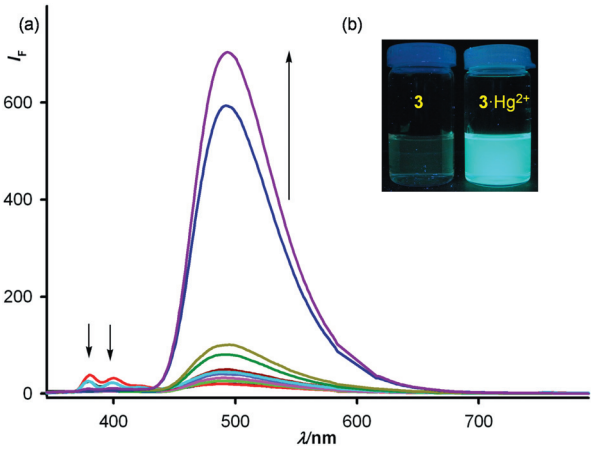

Fig. 3 (a) Changes in the fluorescence emission spectrum of **3** ($c = 1 \times 10^{-5}$ M) in CH_3CN–EtOH–H_2O (65 : 25 : 10) – HEPES mixed buffer solution (pH = 7.4, 20×10^{-3} M HEPES) upon titration with $Hg(OTf)_2$: the initial (black) is that of **3** and the final one (deep purple), after addition of 0.5 equiv. of $Hg(OTf)_2$ ($c = 1 \times 10^{-2}$ M in CH_3CN). Emission is monitored at λ_{ex} = 300 nm. (b) Visual changes observed in the fluorescence of CH_3CN–EtOH–H_2O (65 : 25 : 10) solutions of **3** (left) and after addition of $Hg(OTf)_2$ (right).

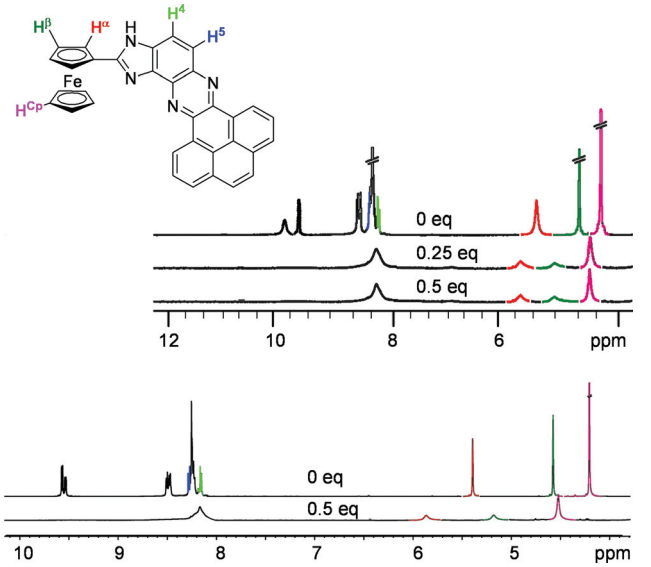

Fig. 4 ^1H NMR titration of 3 in DMSO-d_6 (top) and DMF-d_7 (bottom), upon addition of aliquots of $Hg(OTf)_2$ until 0.5 equiv. was reached.

Binding assays, carried out in the above mentioned mixed aqueous–organic solution, using the method of continuous variations (Job's plot) are consistent with a 2 : 1 (receptor : metal) binding stoichiometry, and from the fluorescence binding isotherm the global association constant was calculated to be $\beta = 1.57 \times 10^{10}$ M^{-2}. The detection limit, calculated as three times the standard deviation of the background noise, was found to be 1.52×10^{-6} M (ESI†).

The binding stoichiometry proposed from absorption and fluorescent data was further confirmed by electrospray mass spectrometry. The ESI-MS spectrum of receptor **3** in the presence of Hg^{2+} ions displays a peak at *m*/*z* 1257.2 corresponding to the 2 : 1 complex. Relative abundances of the isotope peak patterns are in good agreement with the corresponding simulated peak pattern (ESI†).

For the reported constant to be taken with confidence we have proved the reversibility of the complexation process by carrying out the following experimental test: 0.5 equiv. of $Hg(CF_3SO_3)_2$ was added to a solution of the receptor **3** in CH_2Cl_2 to obtain the complexed [$\mathbf{3}_2$·Hg^{2+}], whose OSWV voltammogram and UV-vis spectra were recorded. The solution CH_2Cl_2 of the complex was washed several times with H_2O. The organic layer was dried and the optical spectrum and DPV voltammogram were recorded and they were found to be the same as that of the free receptor **3**. Afterwards, 0.5 equiv. of $Hg(CF_3SO_3)_2$ was added to this solution and the initial UV-vis spectrum, and OSWV voltammogram of the complex [$\mathbf{3}_2$·Hg^{2+}] were fully recovered together. This experiment was carried out over several cycles, and the optical spectrum was recorded after each step, thus demonstrating the high degree of reversibility of the complexation–decomplexation process (ESI†).

The interference in the selective detection of Hg^{2+} carried out both in CH_3CN–EtOH (7 : 3) and in the mixed aqueous–organic solutions [CH_3CN–EtOH–H_2O (65 : 25 : 10)] of receptor **3**, from the other metal cations tested, was also studied by using cross-selectivity experiments. Thus, addition of 1 equiv. of Li^+, Na^+, K^+, Ca^{2+}, Mg^{2+}, Cd^{2+}, Ni^{2+}, Zn^{2+} or Pb^{2+} cations in CH_3CN to 1 equiv. of the receptor **3** in CH_3CN–EtOH–H_2O did not give any optical response. However, further addition of 0.5 equiv. of Hg^{2+} to the above mentioned solutions gave identical optical response to that observed upon addition of 0.5 equiv. of Hg^{2+} to a solution containing only 1 equiv. of the receptor **3** and which is free of the other metal cations (ESI†). These results clearly demonstrate that this receptor has excellent affinity for Hg^{2+} over those ions.

^1H NMR experiments in both DMSO-d_6 and DMF-d_7 were also performed to study the recognition process of receptor **3** with Hg^{2+} (Fig. 4). In the free ligand, and using DMF-d_7 as solvent, four different doublets and two multiplets appear, associated to the protons within the pyrene moiety fused to the phenazine ring. Moreover, two additional doublets at δ = 8.27 ppm and δ = 8.16 ppm assigned to the H5 and H4 of the free receptor **3** have also been detected as well as a singlet at δ = 14.31 ppm due to the NH group. Finally, three different singlets at δ: 4.20, 4.58 and 5.39 ppm are also shown. These are due to the five protons (δ = 4.20 ppm), and to the 2Hα (δ = 4.58 ppm) and 2Hβ (δ = 5.39 ppm) protons present within the unsubstituted and monosubstituted Cp rings, respectively, of the ferrocene subunit. The most remarkable features observed during the formation of the 2 : 1 complex with Hg^{2+} metal cations are the downfield shifting of the signals corresponding to the Hα ($\Delta\delta$ = 0.25 ppm in DMSO-d_6 and 0.47 ppm in DMF-d_7), Hβ ($\Delta\delta$ = 0.43 ppm in DMSO-d_6 and 0.60 ppm in DMF-d_7) and those of the unsubstituted Cp ring ($\Delta\delta$ = 0.21pm in DMSO-d_6 and 0.32pm in DMF-d_7). Moreover, the signals attributed to the H5 and H4 protons are upshifted but now are embedded in the broad multiplet containing all the aromatic protons.

To gain further insights into the binding mode of receptor **3** and Hg^{2+} metal cations, DFT calculations have also been carried out. We selected a simplified model ligand **4** of ferrocene–imidazobenzo- (instead of phenanthro-) phenazine type that has two

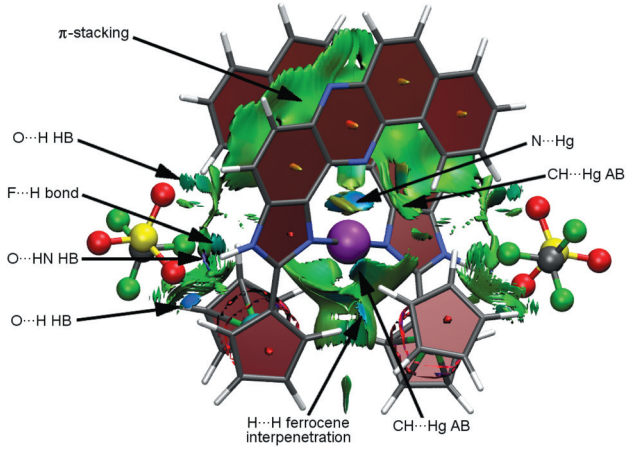

Fig. 5 Calculated (B3LYP-D/def2-TZVP-ecp) structure for the most stable C_2-symmetric [**4**$_2$·Hg(TfO)$_2$] model complex. NCI surfaces have been added to highlight non-covalent interactions. The s = 0.5 au isosurface is colored according to a BGR (blue–green–red) scheme over the range $-0.03 < \text{sign}(\lambda_2)F < 0.03$ au: blue indicates strong attraction, green indicates very weak interaction, and red indicates strong repulsion.

fused benzene rings less (removing two of the "outer" benzene rings), yet features the essential binding and structural framework. Assessment of binding strengths has been achieved within the framework of Bader's atoms-in-molecules (AIM) theory[18] by computing the electron density at the respective bond critical points (BCP), as well as by Wiberg's bond indices (WBI)[19] and Mayer's bond orders (MBO).[20] We have also resorted to NCI (non-covalent interactions) visualization index, which is based on the electron density and its derivatives and enables identification of both stabilizing and de-stabilizing non-covalent interactions.[21] The most stable C_2-symmetric complex shows a well defined receptor-separated ion pair type structure (Fig. 5), sketched as [(TfO)·**4**·Hg·**4**·(OTf)]. Thus, the weakly basic TfO$^-$ anions bind to the imidazole NH groups ($d_{O\cdots HN}$ = 1.602 Å, $WBI_{O\cdots HN}$ = 0.108, $MBO_{O\cdots HN}$ = 0.210, $\rho(\mathbf{r_C})_{O\cdots HN}$ = 5.69 × 10^{-2} e/a_0^3; d_{N-H} = 1.052 Å, WBI_{N-H} = 0.641, MBO_{N-H} = 0.826, $\rho(\mathbf{r_C})_{N-H}$ = 29.66 × 10^{-2} e/a_0^3), these hydrogen bonds (HB) strengthening the ligand–metal bonds (d_{N-Hg} = 2.047 Å, WBI_{N-Hg} = 0.386, MBO_{N-Hg} = 0.555, $\rho(\mathbf{r_C})_{N-Hg}$ = 11.90 × 10^{-2} e/a_0^3). The essentially linear discoordination around the Hg^{2+} cation by two imidazole-type N atoms belonging to two different ligand units (N–Hg–N = 177.6°) approaches the respective large fused aromatic scaffolds (even larger in the actual ligand **3**). An small distortion at the imidazole rings allows parallel arrangement of both aromatic planes (distance between the middle point of the eighteen heavy atoms of one benzoquinoxaline moiety to the other benzoquinoxaline mean plane: 3.130 Å) giving rise to an extensive π-stacking interaction (ΣWBI = 0.301, $\Sigma\rho(\mathbf{r_C})$ = 6.12 × 10^{-2} e/a_0^3, ε_{aver} = 4.549), highlighted in Fig. 5 as a continuous green (weak) NCI surface. At the imidazole edge, the ferrocenyl groups are partially interpenetrated (the non-interpenetrated conformer was found to be 8.2 kcal mol^{-1} less stable at the optimization level) with a pair of short CH···Fe contacts ($d_{H\cdots Fe}$ = 3.089 Å) as well as H···H interferrocene bonding interactions making the overall structure stiffer. Furthermore, such structural features could explain the above mentioned significant downfield shift of the ferrocene ^{1}H NMR resonances in the complex. The coordination sphere around mercury is complemented by a set of three pairs of additional weak interactions, one of them involving the pyridine-type nitrogen atoms (d_{N-Hg} = 2.886 Å, WBI_{N-Hg} = 0.083, MBO_{N-Hg} = 0.121, $\rho(\mathbf{r_C})_{N-Hg}$ = 2.25 × 10^{-2} e/a_0^3). Moreover, the unsubstituted ferrocenyl Cp rings locate two H ring protons pointing close to the Hg^{2+} cation, which surround the metal with a weak NCI isosurface ($d_{H\cdots Hg}$ = 2.895 Å, $WBI_{H\cdots Hg}$ = 0.010, $MBO_{H\cdots Hg}$ < 0.1, $\rho(\mathbf{r_C})_{H\cdots Hg}$ = 1.02 × 10^{-2} e/a_0^3) also spanning the interpenetration between ferrocene units. Similarly, the rigid benzophenazine frameworks feature two H ring protons pointing towards the central cation (C–H···Hg angle 137.8°) allowing formation of anagostic[22] bonds, which give rise to strong blue NCI surfaces ($d_{H\cdots Hg}$ = 3.106 Å, $WBI_{H\cdots Hg}$ = 0.009, no BCP). Additional secondary O···H and F···H contacts also reinforce the binding to every peripheral TfO$^-$ anion (ΣWBI = 0.123, $\Sigma\rho(\mathbf{r_C})$ = 6.58 × 10^{-2} e/a_0^3). Moreover, extensive dispersive interactions are found between the peripheral triflate anions and the outer part of the ferrocenyl–imidazobenzophenazine ligand that add to the rigidity of the structure (ESI†).

Conclusions

We describe the preparation and sensing properties of a ferrocene-substituted imidazophenenthrophenazine ring system. This receptor acts as a selective molecular probe of Hg^{2+} in aqueous environment through three different channels: electrochemical, colorimetric and fluorescent. An anodic shift of the ferrocene–ferrocenium redox couple ($\Delta E_{1/2}$ = 240 mV) and a progressive red-shift ($\Delta\lambda$ = 17 nm) of the low energy band in its absorption spectrum is observed, in the presence of Hg^{2+} cations. In addition, the emission spectrum is perturbed after addition of Hg^{2+} cations and an intense and structureless red-shift emission band ($\Delta\lambda$ = 92 nm) appeared along with an increase of the intensity of such emission band (CHEF = 77). In the presence of Li$^+$, Na$^+$, K$^+$, Ca^{2+}, Mg^{2+}, Cd^{2+}, Ni^{2+}, Zn^{2+} or Pb^{2+} cations the receptor did not give any fluorescent or electrochemical response although it behaves as colorimetric sensor for Zn^{2+} or Pb^{2+} metal cations. In summary, the results reported here clearly demonstrate that this receptor has excellent affinity for Hg^{2+} over the other cations tested. The combined ^{1}H NMR data of the complex and the theoretical calculation suggest the proposed binding coordination mode.

Experimental

General methods

Melting points were determined on a hot-plate melting point apparatus and are uncorrected. ^{1}H- and ^{13}C-NMR spectra were recorded at 400 and 100 MHz, respectively. Chemical shifts refer to signals of tetramethylsilane in the case of ^{1}H and ^{13}C spectra. The following abbreviations are used to represent the multiplicity of the signals: s (singlet), d (doublet), dd (double doublets), m (multiplet), Cq (quaternary carbon atom).

The set of metal cations used were added as perchlorate (Li$^+$, K$^+$, Mg^{2+}, Ni^{2+}, Cd^{2+} and Pb^2) (*WARNING: perchlorate salts are hazardous because of the possibility of explosion; only small amounts of this material should be handled and with great*

caution) or triflate (Na^+, Ca^{2+}, Cu^{2+}, Zn^{2+} and Hg^{2+}) salts solved in CH_3CN at the concentrations described below for each of the techniques used.

UV-vis spectra were carried out in a UV-vis-NIR spectrophotometer using a dissolution cell of 10 mm path. The samples were solved in the appropriate solvent ($c = 5 \times 10^{-5}$ M, see figure captions) and the spectra were recorded with the spectra background corrected before and after the sequential additions of aliquots of 0.1 equiv. of cations in CH_3CN ($c = 2.5 \times 10^{-2}$ M). The association constants were obtained using the computer program Specfit/32 Global Analysis System[16].

Fluorescence spectra were carried out in a fluorescence spectrophotometer using a fluorescence cell 10 mm ($c \approx 1 \times 10^{-5}$ M in the appropriate solvent, as stated in the corresponding figure captions). Before recording the spectra, the samples were deoxygenated to remove fluorescence quenching *via* oxygen by bubbling nitrogen for at least 10 min. All the spectra were recorded before and after the sequential additions of aliquots of 0.1 equiv. of a solution of cations in CH_3CN ($c = 1 \times 10^{-2}$ M). Quantum yield values were measured with respect to an ethanolic solution of anthracene as standard ($\Phi = 0.27 \pm 0.01$),[23] using the equation $\Phi_x/\Phi_s = (S_x/S_s)\ [(1-10^{-As})/(1-10^{-Ax})]^2(n_s^2/n_x^2)$ where x and s indicate the unknown and standard solution, respectively, Φ is the quantum yield, S is the area under the emission curve, A is the absorbance at the excitation wavelength and n is the index of refraction.

CV and OSWV techniques were performed with a conventional three-electrode configuration consisting of platinum working and auxiliary electrodes and a Ag–AgCl reference electrode. The experiments were carried out with a $\approx 10^{-4}$ M solution of sample in CH_3CN containing 0.1 M $(n\text{-}C_4H_9)_4PF_6$ ($TBAPF_6$) as supporting electrolyte. All the potential values reported are relative to the decamethylferrocene (DMFc) couple at room temperature. Deoxygenation of the solutions was achieved by bubbling nitrogen for at least 10 min and the working electrode was cleaned after each run. The cyclic voltammograms were recorded with a scan rate increasing from 0.05 to 1.00 V s^{-1}, while the OSWV were recorded at a scan rate of 100 mV s^{-1} with a pulse high of 10 mV and a step time of 50 ms. Typically, receptor (1×10^{-4} M) was dissolved in CH_3CN (5 mL) and $TBAPF_6$ (base electrolyte) (0.190 g) added. The guest under investigation was then added as a 2.5×10^{-2} M solution in CH_3CN using a microsyringe whilst the cyclic voltammetric properties of the solution were monitored. DMFc was used as an external reference both for potential calibration and for reversibility criteria.

Synthesis of 2-ferrocenyl-3*H*-imidazo[4,5-h]phenanthro[4,5-abc] phenazine, 3

To a solution of 2-ferrocenyl-4,5-diamino-1*H*-benzo[*d*]imidazole (0.20 g, 0.60 mmol) in nitrobenzene (10 mL), pyrene-4,5-dione (0.14 g, 0.60 mmol) and acetic acid (0.5 mL) were added. The mixture was stirred at 60 °C overnight and then neutralized to pH 7 with a $NaHCO_3$ solution. The reaction mixture was poured into H_2O (50 mL), and the solution was extracted with $CHCl_3$ (2×50 mL). The organic phase was dried over anhydrous Na_2SO_4 and the solvent was removed under reduced pressure to afford a brown residue. Column chromatography (dichloromethane–hexane–methanol (9 : 1 : 0.5)) gave the pure product as an orange solid in 35% yield (0.9 g). Mp 230–232 °C. Found: C, 75.29; H, 3.61; N, 10.36. Calc. for $C_{33}H_{20}FeN_4$: C, 75.01; H, 3.82; N, 10.60%. δ_H (400 MHz, DMF-d_7) 4.20 (5H, s), 4.58 (2H, s), 5.39 (2H, s), 8.16 (1H, d, $J = 8.8$ Hz); 8.25 (2H, m), 8.22 (2H, m), 8.27 (1H, d, $J = 8.8$ Hz), 8.47 (1H, d, $J = 7.6$ Hz), 9.50 (1H, d, $J = 7.6$ Hz), 9.53 (1H, d, $J = 7.6$ Hz), 9.57 (1H, dd, $J = 0.8$; 7.6 Hz), 14.30 (NH, s); δ_C (100 MHz, DMF-d_7) 67.9 (CH), 68.2 (CH), 69.9 (CH), 70.45 (CH), 75.11 (Cq), 123.3 (CH), 123.5 (CH), 123.7 (CH), 124.9 (CH), 125.6 (Cq), 126.0 (Cq), 127.3 (CH), 127.6 (CH), 127.7 (CH), 127.9 (CH), 129.1 (CH), 129.5 (CH), 129.9 (Cq), 130.0 (Cq), 130.1 (Cq), 132.0 (Cq), 132.7 (Cq), 140.6 (Cq), 140.7 (Cq), 141.3 (Cq), 145.1 (Cq), 155.1 (Cq); *m/z* (EI) 528 (M^+, 100), 264 (85).

Computational details

Quantum chemical calculations were performed with the ORCA electronic structure program package.[24] All geometry optimizations were run with tight convergence criteria, using the B3LYP[25] functional together with the new efficient RIJCOSX algorithm[26] and the def2-TZVP(-f) basis set.[27] For Hg atoms the [OLD-SD(60,MDF)] effective core potential[28] (ECP) was used. In all optimizations a damped semiempirical correction accounting for the major part of the contribution of dispersion forces to the energy was included[29] and denoted with suffix D after the name of the functional (B3LYP-D). From these gas-phase optimized geometries all reported data were obtained by means of single-point (SP) calculations using the full def2-TZVP basis set. Reported energies are uncorrected for the zero-point vibrational term. The topological analysis of the electronic charge density was conducted using the AIM2000 software[30] and the wavefunctions generated with the def2-TZVP basis set and the Gaussian09 software package.[31] Computations for NCI (non-covalent interactions) have been carried out with the NCIplot program[32] and using the electron densities obtained with the B3LYP functional and 6–31G basis sets on all the atoms except for Hg, where SDD basis set and pseudopotentials were used.[33] Fig. 5 and Fig. S25–S27† were generated with VMD 1.8.7.[34]

NCI methodology is based on the analysis of the reduced density gradient (RDG, s) with respect to the density. When a weak interaction is taking place, there is a crucial change in the RDG in between the atoms involved (inter or intramolecular). Peaks appear in the *s vs.* ρ plot, which correspond in 3D to the regions of non-covalent regions (steric clashes, van der Waals, hydrogen bonds, *etc.*). Further analysis of the peaks is needed in order to be able to assign their nature. The density values of the peaks are a good indicator of the interaction strength. However, both attractive and repulsive interactions (*i.e.* hydrogen-bonding and steric crowding) appear in the same region of density/RDG space. To distinguish between attractive and repulsive interactions, we must consider second derivatives of the density. Whereas bonding interactions, such as hydrogen bonds, are characterized by an accumulation of density perpendicular to the bond and a negative second eigenvalue, non-bonding interactions, such as steric crowding, result in a positive second eigenvalue. Extremely weak interactions, such as van der Waals

or stacking, are characterized by a negligible density overlap that gives rise to a second eigenvalue very close to zero.

Acknowledgements

We gratefully acknowledge the financial support from MICINN-Spain, Project CTQ2008-01402 and Fundación Séneca (Agencia de Ciencia y Tecnología de la Región de Murcia) project 04509/GERM/06 (Programa de Ayudas a Grupos de Excelencia de la Región de Murcia, Plan Regional de Ciencia y Tecnología 2007/2010). We also wish to thank the Supercomputation Center at Fundación Parque Científico de Murcia (FPCMur) for their technical support and the computational resources used in the supercomputer *Ben-Arabí*. JCG thanks MICINN-Spain for a postdoctoral mobility grant (EDU/2253/2010).

References

1 (*a*) W. Sekowski, L. H. Malkas, Y. Wei and R. J. Hickey, *Toxicol. Appl. Pharmacol.*, 1997, **145**, 268–276; (*b*) World Health Organization, *Environmental Health Criteria 118: Inorganic Mercury*, World Health Organization, Geneva, 1991.

2 (*a*) T. W. Clarkson, L. Magos and G. J. Myers, *N. Engl. J. Med.*, 2003, **349**, 1731–1737; (*b*) F. M. M. Morel, A. M. L. Kraepiel and M. Amyot, *Annu. Rev. Ecol. Syst.*, 1998, **29**, 543–566.

3 *Guidelines for Drinking Water Quality*, World Health Organization, Geneva, 3rd edn, 2004, p. 188.

4 For a recent review, see: E. M. Nolan and S. J. Lippard, *Chem. Rev.*, 2008, **108**, 3443–3480.

5 (*a*) A. P. de Silva, H. Q. N. Gunaratne, T. Gunnlaugsson, A. J. M. Huxley, C. P. McCoy, J. T. Rademacher and T. E. Rice, *Chem. Rev.*, 1997, **97**, 1515–1566; (*b*) B. Valeur and I. Leray, *Coord. Chem. Rev.*, 2000, **205**, 3–40.

6 For selected recent examples, see: (*a*) A. Caballero, R. Martinez, V. Lloveras, I. Ratera, J. Vidal-Gancedo, K. Wurst, A. Tárraga, P. Molina and J. Veciana, *J. Am. Chem. Soc.*, 2005, **127**, 15666–15667; (*b*) E. M. Nolan and S. J. Lippard, *J. Am. Chem. Soc.*, 2003, **125**, 14270–14271; (*c*) J. V. Ros-Lis, M. D. Marcos, R. Martinez-Mañez, K. Rurack and J. Soto, *Angew. Chem., Int. Ed.*, 2005, **44**, 4405–4407; (*d*) I. B. Kim and U. H. F. Bunz, *J. Am. Chem. Soc.*, 2006, **128**, 2818–2819; (*e*) I. B. Kim, B. Erdogan, J. N. Wilson and U. H. F. Bunz, *Chem.–Eur. J.*, 2004, **10**, 6247–6254; (*f*) S. J. Ou, Z. H. Lin, C. Y. Duan, H. T. Zhang and Z. P. Bai, *Chem. Commun.*, 2006, 4392–4394; (*g*) J. B. Wang and H. Qian, *Org. Lett.*, 2006, **8**, 3721–3724; (*h*) R. Martínez, F. Zapata, A. Caballero, A. Espinosa, A. Tárraga and P. Molina, *Org. Lett.*, 2006, **8**, 3235–3238; (*i*) A. Ono and H. Togashi, *Angew. Chem., Int. Ed.*, 2004, **43**, 4300–4302; (*j*) S. Yoon, A. E. Albers, A. P. Wong and C. J. Chang, *J. Am. Chem. Soc.*, 2005, **127**, 16030–16031; (*k*) X. J. Zhu, S. T. Fu, W. K. Wong, H. P. Guo and W. Y. Wong, *Angew. Chem., Int. Ed.*, 2006, **45**, 3150–3154; (*l*) C. Diez-Gil, R. Martínez, I. Ratera, A. Tárraga, P. Molina and J. Veciana, *J. Mater. Chem.*, 2008, **18**, 1997–2002; (*m*) M. Yuan, W. Zhou, X. Liu, M. Zhu, J. Li, X. Yin, H. Zheng, Z. Zuo, C. Ouyang, H. Liu, Y. Li and D. Zhu, *J. Org. Chem.*, 2008, **73**, 5008–5014; (*n*) D. Wu, W. Huang, Z. Lin, C. Duan, C. He, S. Wu and D. Wang, *Inorg. Chem.*, 2008, **47**, 7190–7201; (*o*) W. Huang, C. Song, C. He, G. Lv, X. Hu, X. Zhu and C. Duan, *Inorg. Chem.*, 2009, **48**, 5061–5072; (*p*) X. Chen, S.-W. Nam, M. J. Jou, Y. Kim, S.-J. Kim, S. Park and J. Yoon, *Org. Lett.*, 2008, **10**, 5235–5238; (*q*) M. Suresh, S. Mishra, S. K. Mishra, E. Suresh, A. K. Mandal, A. Shrivastav and A. Das, *Org. Lett.*, 2009, **11**, 2740–2743; (*r*) H. F. Shi, S. J. Liu, H. B. Sun, W. J. Xu, Z. F. An, J. Chen, S. Sun, X. M. Lu, Q. Zhao and W. Huang, *Chem.–Eur. J.*, 2010, **16**, 12158–12167; (*s*) Y. H. Lau, J. R. Price, M. H. Todd and P. T. Rutledge, *Chem.–Eur. J.*, 2011, **17**, 2850–2858; C. Chen, R. Wang, L. Guo, N. Fu, H. Dong and Y. Yuan, *Org. Lett.*, 2011, **13**, 1162–1165.

7 P. Molina, A. Tárraga and A. Caballero, *Eur. J. Inorg. Chem.*, 2008, 3401–3417.

8 (*a*) T. Romero, A. Caballero, A. Espinosa, A. Tárraga and P. Molina, *Dalton Trans.*, 2009, 2121–2129; (*b*) F. Zapata, A. Caballero, A. Espinosa, A. Tárraga and P. Molina, *J. Org. Chem.*, 2009, **74**, 4787–4796; (*c*) F. Zapata, A. Caballero, A. Espinosa, A. Tárraga and P. Molina, *Inorg. Chem.*, 2009, **48**, 11566–11575; (*d*) T. Romero, A. Caballero, A. Tárraga and P. Molina, *Org. Lett.*, 2009, **11**, 3466–3469; (*e*) F. Zapata, A. Caballero, A. Espinosa, A. Tárraga and P. Molina, *Dalton Trans.*, 2010, **39**, 5429–5431.

9 (*a*) M. Alfonso, A. Sola, A. Caballero, A. Tárraga and P. Molina, *Dalton Trans.*, 2009, 9653–9658; (*b*) M. Alfonso, A. Tárraga and P. Molina, *Dalton Trans.*, 2010, **39**, 8637–8645; (*c*) M. Alfonso, A. Tárraga and P. Molina, *J. Org. Chem.*, 2011, **76**, 939–947.

10 J. Hu, D. Zhang and F. W. Harris, *J. Org. Chem.*, 2005, **70**, 707–708.

11 OSWV technique has been employed to obtain well-resolved potential information, while the individual redox processes are poorly resolved in the CV experiments in which individual $E_{1/2}$ potentials cannot be easily or accurately extracted from these data; (*a*) B. R. Serr, K. A. Andersen, C. M. Elliot and O. P. Anderson, *Inorg. Chem.*, 1988, **27**, 4499–4504; (*b*) D. E. Richardson and H. Taube, *Inorg. Chem.*, 1981, **20**, 1278–1285.

12 N. G. Connelly and W. E. Geiger, *Chem. Rev.*, 1996, **96**, 877–910.

13 (*a*) S. R. Marder, J. W. Perry and B. G. Tiemann, *Organometallics*, 1991, **10**, 1896–1901; (*b*) B. J. Coe, C. J. Jones, J. A. McCleverty, D. Bloor and G. J. Cross, *J. Organomet. Chem.*, 1994, **464**, 225–232; (*c*) T. J. Mller, A. Netz and M. Ansorge, *Organometallics*, 1999, **18**, 5066–5074; (*d*) J. D. Carr, S. J. Coles, M. B. Asan, M. B. Hurthouse, K. M. A. Malik and J. H. R. Tucker, *J. Chem. Soc., Dalton Trans.*, 1999, 57–62.

14 (*a*) G. L. Geoffroy and M. S. Wrighton, *Organometallic Photochemistry*, Academic Press, New York, 1979; (*b*) H. B. Gray, Y. S. Sohn and N. Hendrickson, *J. Am. Chem. Soc.*, 1971, **93**, 3603–3612.

15 (*a*) S. Barlow, H. E. Bunting, C. Ringham, J. C. Green, G. U. Bublitz, S. G. Boxer, J. W. Perry and S. R. Marder, *J. Am. Chem. Soc.*, 1999, **121**, 3715–3723; (*b*) G. E. Southhard and M. D. Curtis, *Organometallics*, 2001, **20**, 508–522; (*c*) K. Naka, T. Uemura and Y. Chujo, *Macromolecules*, 2000, **33**, 6965–6969.

16 Specfit/32 Global Analysis System, 1994–2004 Spectrum Software Associates (SpecSoft@compuserve.com), which was acquired from Biologic SA (www.bio-logic.info) in January 2005.

17 CHEF is defined as the I_{max}/I_0, where I_{max} corresponds to the maximum emission intensity of the receptor–metal complex, while I_0 is the maximum emission intensity of the free receptor. For recent and relevant examples of heavy and transition metal cation (HTM) chemosensors based on the chelation-enhanced fluorescence (CHEF) see: (*a*) R. Martínez, A. Espinosa, A. Tárraga and P. Molina, *Tetrahedron*, 2010, **66**, 3662–3667; (*b*) Y. Ding, Y. Xie, X. Li, J. P. Hill, W. Zhang and W. Zhu, *Chem. Commun.*, 2011, **47**, 5431–5433.

18 (*a*) R. F. W. Bader, *Atoms in Molecules: A Quantum Theory*, Oxford University Press, Oxford, 1990; (*b*) R. F. W. Bader, *Chem. Rev.*, 1991, **91**, 893–928; (*c*) C. F. Matta and R. J. Boyd, in *The Quantum Theory of Atoms in Molecules*, ed. C. F. Matta and R. J. Boyd, Wiley-VCH, New York, 2007, pp. 1–34.

19 K. Wiberg, *Tetrahedron*, 1968, **24**, 1083–1096.

20 (*a*) I. Mayer, *Chem. Phys. Lett.*, 1983, **97**, 270–274; (*b*) I. Mayer, *Int. J. Quantum Chem.*, 1984, **26**, 151–154; (*c*) I. Mayer, *Theor. Chim. Acta*, 1985, **67**, 315–322; (*d*) I. Mayer, in *Modelling of Structure and Properties of Molecules*, ed. Z. B. Maksic, John Wiley & Sons, New York, Chichester, Brisbane, Toronto, 1987; (*e*) A. J. Bridgeman, G. Cavigliasso, L. R. Ireland and J. Rothery, *J. Chem. Soc., Dalton Trans.*, 2001, 2095–2108.

21 (*a*) E. R. Johnson, S. Keinan, P. Mori-Sánchez, J. Contreras García, A. J. Cohen and W. Yang, *J. Am. Chem. Soc.*, 2010, **132**, 6498–6506; (*b*) J. Contreras García, E. R. Johnson, S. Keinan, R. Chaudret, J.-P. Piquemal, D. N. Beratan and W. Yang, *J. Chem. Theory Comput.*, 2011, **7**, 625–632.

22 Anagostic M–H–C bonds are best described as a "hydrogen bond" involving a 3-centre–4-electron orbital interaction with an electrostatic contribution in which the metal serves as a hydrogen bond acceptor. They are characterized by relatively long M···H distances (≫2.3–3.2 Å) and large M–H–C angles (≫110–170°).

23 W. R. Dawson and M. W. Windsor, *J. Phys. Chem.*, 1968, **72**, 3251–3260.

24 F. Neese, *ORCA – an* ab initio*, density functional and semiempirical program package*, Version 2.8.0, UniversitätBonn, 2010, http://www.thch.uni-bonn.de/tc/orca/.Tight convergence criteria for optimizations in ORCA: energy change 1.0×10^{-6} hartree; maximum gradient 1.0×10^{-4} hartree/a_0; RMS gradient 3.0×10^{-5} hartree/a_0; maximum displacement 1.0×10^{-3} a_0; RMS displacement 6.0×10^{-4} a_0.

25 (*a*) A. D. Becke, *J. Chem. Phys.*, 1993, **98**, 5648–5652; (*b*) C. T. Lee, W. T. Yang and R. G. Parr, *Phys. Rev. B*, 1988, **37**, 785–789.
26 F. Neese, F. Wennmohs, A. Hansen and U. Becker, *Chem. Phys.*, 2009, **356**, 98–109.
27 F. Weigend and R. Ahlrichs, *Phys. Chem. Chem. Phys.*, 2005, **7**, 3297–3305.
28 U. Häussermann, M. Dolg, H. Stoll, H. Preuss, P. Schwerdtfeger and R. M. Pitzer, *Mol. Phys.*, 1993, **78**, 1211–1224. ECP parameters for Hg [OLD-SD(60,MDF)] have been obtained from the pseudopotential library of the Stuttgart/Cologne group at http://www.theochem.uni-stuttgart.de/pseudopotentials/.
29 (*a*) S. Grimme, *J. Comput. Chem.*, 2004, **25**, 1463–1476; (*b*) S. Grimme, *J. Comput. Chem.*, 2006, **27**, 1787–1799.
30 (*a*) *AIM2000 v. 2.0*, designed by F. Biegler-König and J. Schönbohm, 2002, http://www.aim2000.de/; F. Biegler-König, J. Schönbohm and D. J. Bayles, *Comp. Chem.*, 2001, **22**, 545–559; (*b*) F. Biegler-König and J. Schönbohm, *J. Comput. Chem.*, 2002, **23**, 1489–1494.
31 M. J. Frisch, G. W. Trucks, H. B. Schlegel, G. E. Scuseria, M. A. Robb, J. R. Cheeseman, G. Scalmani, V. Barone, B. Mennucci, G. A. Petersson, H. Nakatsuji, M. Caricato, X. Li, H. P. Hratchian, A. F. Izmaylov, J. Bloino, G. Zheng, J. L. Sonnenberg, M. Hada, M. Ehara, K. Toyota, R. Fukuda, J. Hasegawa, M. Ishida, T. Nakajima, Y. Honda, O. Kitao, H. Nakai, T. Vreven, J. A. Montgomery, Jr., J. E. Peralta, F. Ogliaro, M. Bearpark, J. J. Heyd, E. Brothers, K. N. Kudin, V. N. Staroverov, R. Kobayashi, J. Normand, K. Raghavachari, A. Rendell, J. C. Burant, S. S. Iyengar, J. Tomasi, M. Cossi, N. Rega, J. M. Millam, M. Klene, J. E. Knox, J. B. Cross, V. Bakken, C. Adamo, J. Jaramillo, R. Gomperts, R. E. Stratmann, O. Yazyev, A. J. Austin, R. Cammi, C. Pomelli, J. Ochterski, R. L. Martin, K. Morokuma, V. G. Zakrzewski, G. A. Voth, P. Salvador, J. J. Dannenberg, S. Dapprich, A. D. Daniels, O. Farkas, J. B. Foresman, J. V. Ortiz, J. Cioslowski and D. J. Fox, *GAUSSIAN 09 (Revision A.2)*, Gaussian, Inc., Wallingford, CT, 2009.
32 *NCIplot, version 1.1.x*, Department of Chemistry, Duke University, USA, 2011, http://www.chem.duke.edu/~yang/Software/softwareNCI.html; (*a*) E. R. Johnson, S. Keinan, P. Mori-Sánchez, J. Contreras García, A. J. Cohen and W. Yang, *J. Am. Chem. Soc.*, 2010, **132**, 6498–6506; (*b*) J. Contreras García, E. R. Johnson, S. Keinan, R. Chaudret, J.-P. Piquemal, D. N. Beratan and W. Yang, *J. Chem. Theory Comput.*, 2011, **7**, 625–632.
33 (*a*) D. Andrae, U. Haeussermann, M. Dolg, H. Stoll and H. Preuss, *Theor. Chim. Acta*, 1990, **77**, 123–141; (*b*) J. M. L. Martin and A. Sundermann, *J. Chem. Phys.*, 2001, **114**, 3408–3420. ECP parameters for Hg [SD(60,MWB)] have been obtained from the pseudopotential library of the Stuttgart/Cologne group, at http://www.theochem.uni-stuttgart.de/pseudopotentials/.
34 W. Humphrey, A. Dalke and K. Schulten, VMD — Visual Molecular Dynamics, *J. Mol. Graphics*, 1996, **14**, 33–38; home page http://www.ks.uiuc.edu/Research/vmd/.

